Electronic Supplementary Material (ESI) for Organic Chemistry Frontiers.

SUPPORTING INFORMATION

Mechanistic insights into the rhodium catalysed dehydrogenative cycloaddition of cyano-yne-allene substrates

Àlex Díaz-Jiménez,[a] Anna Roglans,[a] Miquel Solà*,[a], Anna Pla-Quintana*,[a]

[a] Institut de Química Computacional i Catàlisi (IQCC) and Departament de Química, Universitat de Girona (UdG), Facultat de Ciències, C/ Maria Aurèlia Capmany, 69, 17003-Girona, Catalunya, Spain.

CONTENTS

1. Computational data 3

2. Comparison of the deformation energy in transition state structures TSA1A2 and TSB1B2 ... 3

3. Study of alternative pathways 4

3.1. Comparison of the deprotonation of A2 and A3 with nitrile insertion on A3. 4

3.2. Comparison of the deprotonation of A2’ and A3’ with nitrile insertion on A3’..... 5

3.3. Comparison of the N protonation versus Cl abstraction in A6..... 7

3.4. Comparison of the Rh-catalyzed versus Et_3N mediated deprotonation of A9..... 8

3.5. Computed energy profile for B pathway. 11

4. Molecular structures of A4, A4’ and substituted allenes A4Ext and A4Int 12

5. Study of the steric difference between the internal and external allene carbons in A4 and A4’ 14

1. Computational data

All DFT data obtained within this study are provided through the following link: https://iochem.udg.edu/browse/handle/100/5173

2. Comparison of the deformation energy in transition state structures TSA1A2 and TSB1B2

Table S1. Deformation energy data for TSA1A2 and TSB1B2

TSA1A2	
ΔE Rhodium fragment	9.1122 kcal/mol
ΔE ene-yne-nitrile fragment	78.5617 kcal/mol
Total value ΔE	87.6740 kcal/mol
TSB1B2	
ΔE Rhodium fragment	6.1193 kcal/mol
ΔE ene-yne-nitrile fragment	85.0384 kcal/mol
Total value ΔE	91.1577 kcal/mol
ΔE TSB1B2 - ΔE TSA1A2	**3.48375 kcal/mol**

Geometry analysis was conducted on the **1a** moiety in **TSA1A2** and **TSB1B2**, revealing that the major deformation of **1a** in **TSB1B2** arises from the strained angles around the former central carbon of the allene. During the oxidative cyclization this central carbon rehybridizes from *sp* to sp^2. In **TSB1B2** the angles around this carbon significantly deviate from the expected 120º for an sp^2 carbon, primarily due to the strained angle in the forming rhodacyclopentene moiety. This strain becomes evident when comparing the angles with those of intermediate **B2**. Conversely, the corresponding deformations around this carbon in **TSA1A2** are notably minor, consistent with the decreased computed deformation energy.

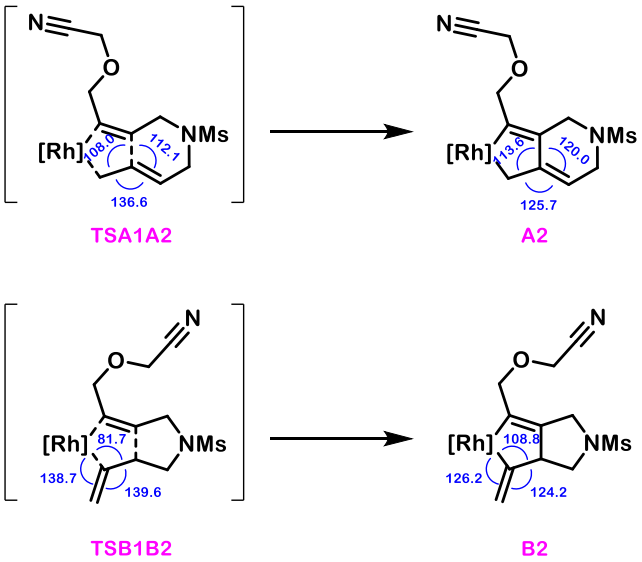

Scheme S1. DFT calculations for the deprotonation of **A2** and **A3** (lines and structures in blue) and comparison with nitrile insertion on **A3** through **TSA3A4.**

3. Study of alternative pathways

3.1. Comparison of the deprotonation of A2 and A3 with nitrile insertion on A3.

Deprotonation from **A2** was found to have an activation energy of 30.6 kcal/mol, which is notably higher than nitride insertion on **A3**, which has an activation energy of 8.8 kcal/mol (Figure S1). The barrier for the deprotonation from **A3** could not be located. However, the **A3_NEt3** adduct has already an energy of 4.5 kcal/mol (Figure S1), only 0.8 kcal/mol lower than **TSA3A4**, and a scan on the C-H distance (Figure S2) showed that the barrier is not lower than 28 kcal/mol letting thus to disregard both options.

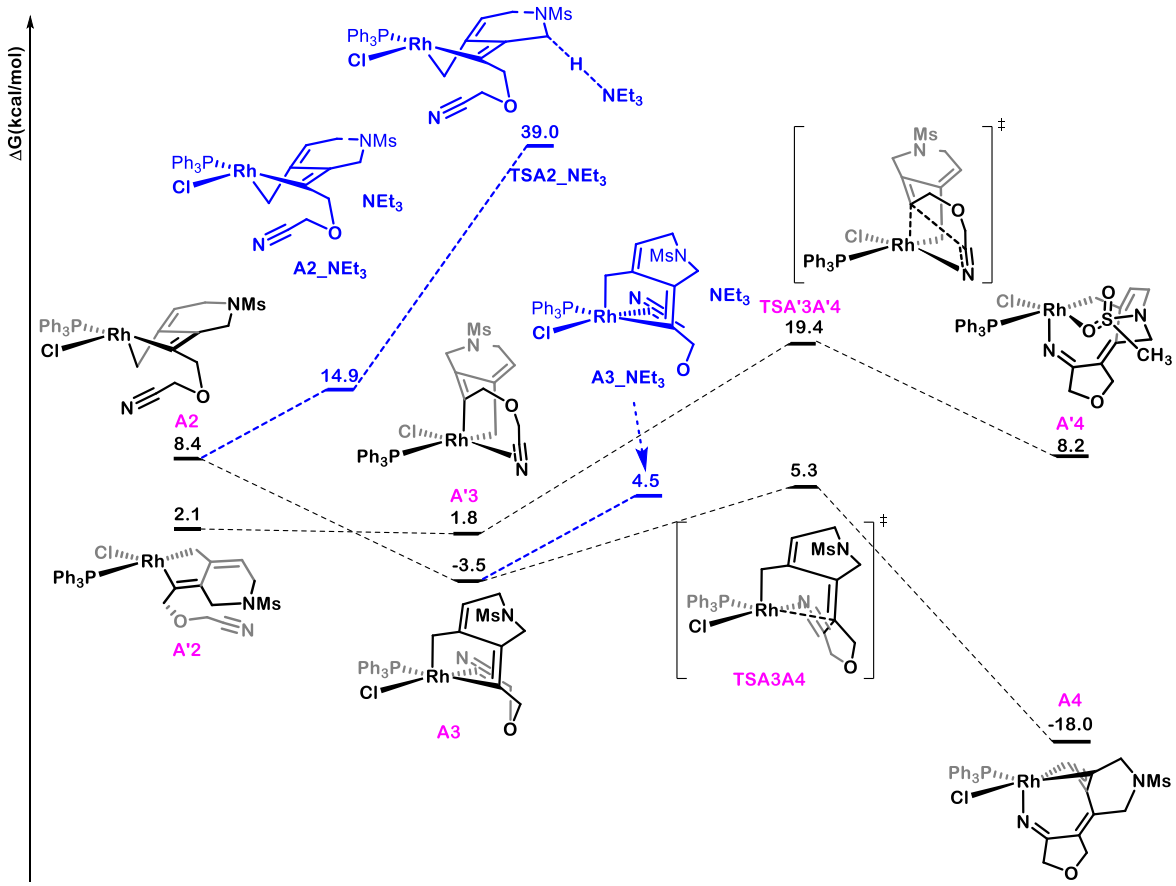

Figure S1. DFT calculations for the deprotonation of **A2** and **A3** (lines and structures in blue) and comparison with nitrile insertion on **A3** through **TSA3A4.**

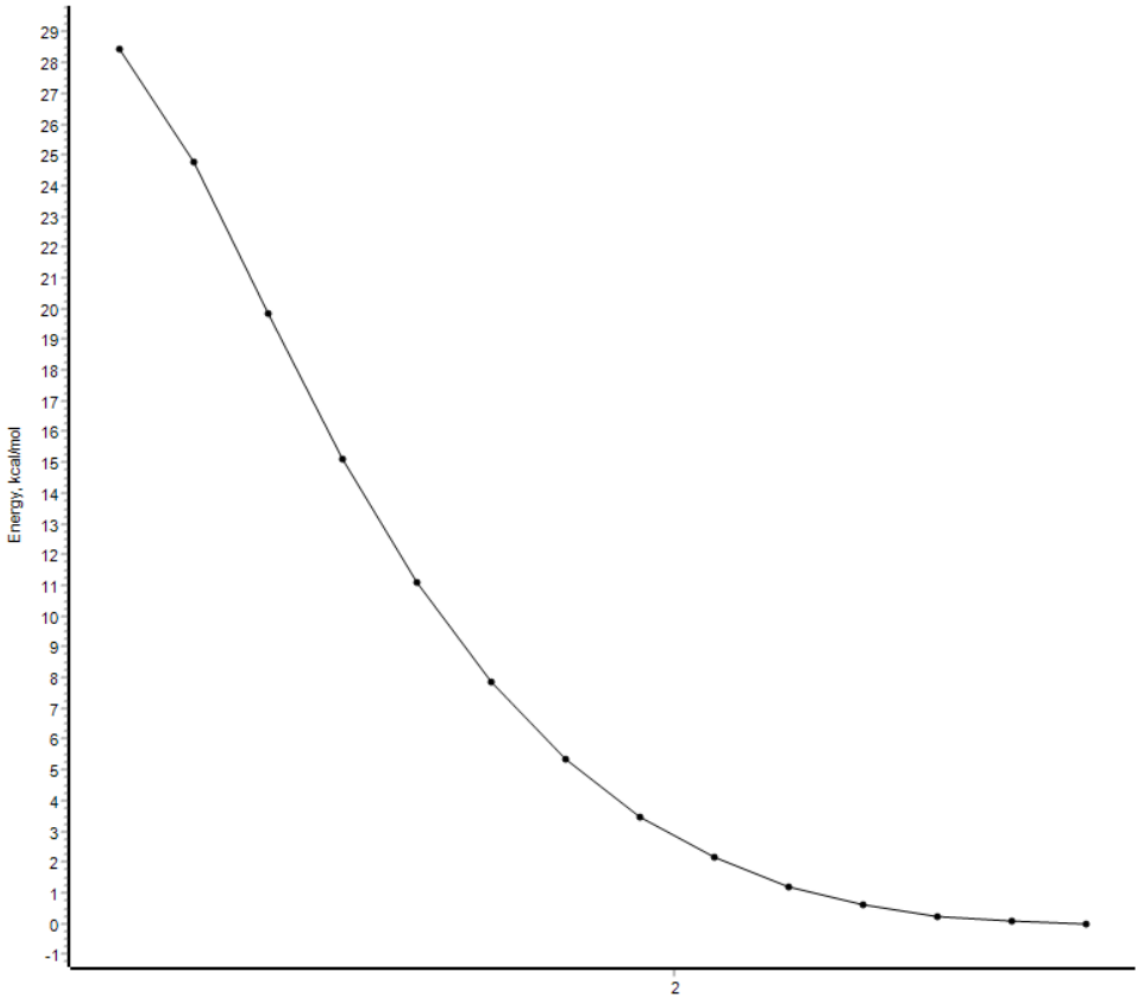

Figure S2. Scan on the C-H distance for the deprotonation of **A3_NEt3.**

3.2. Comparison of the deprotonation of A2' and A3' with nitrile insertion on A3'.

Deprotonation from A2' was found to have an activation energy of 22.3 kcal/mol, which is higher than nitride insertion on A3', which has an activation energy of 17.6 kcal/mol (Figure S3). The barrier for the deprotonation from A3' could not be located. However, the A3'_Et3N adduct has already an energy of 11.7 kcal/mol (Figure S3), and a scan on the C-H distance (Figure S4) showed that the barrier is not lower than 30 kcal/mol letting us again to disregard both options.

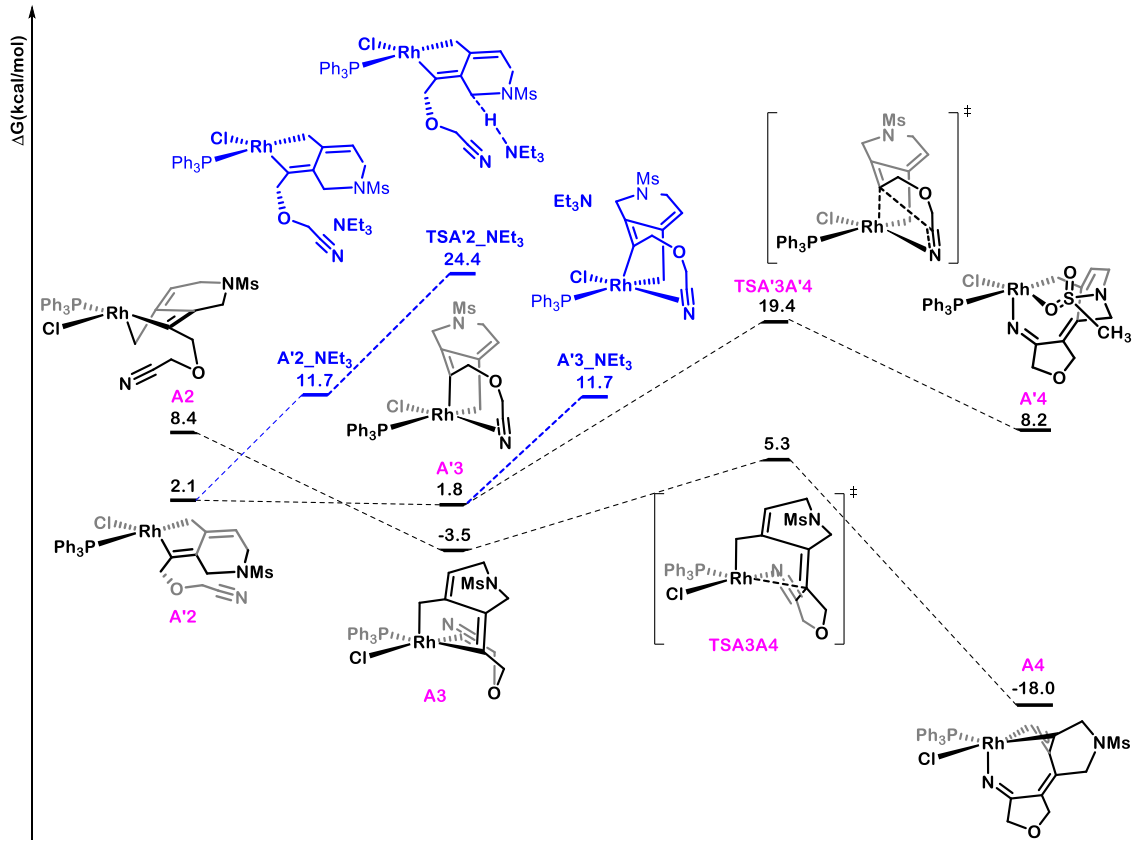

Figure S3. DFT calculations for the deprotonation of **A2'** and **A3'** (lines and structures in blue) and comparison with nitrile insertion on **A3'** through **TSA3'A4'.**

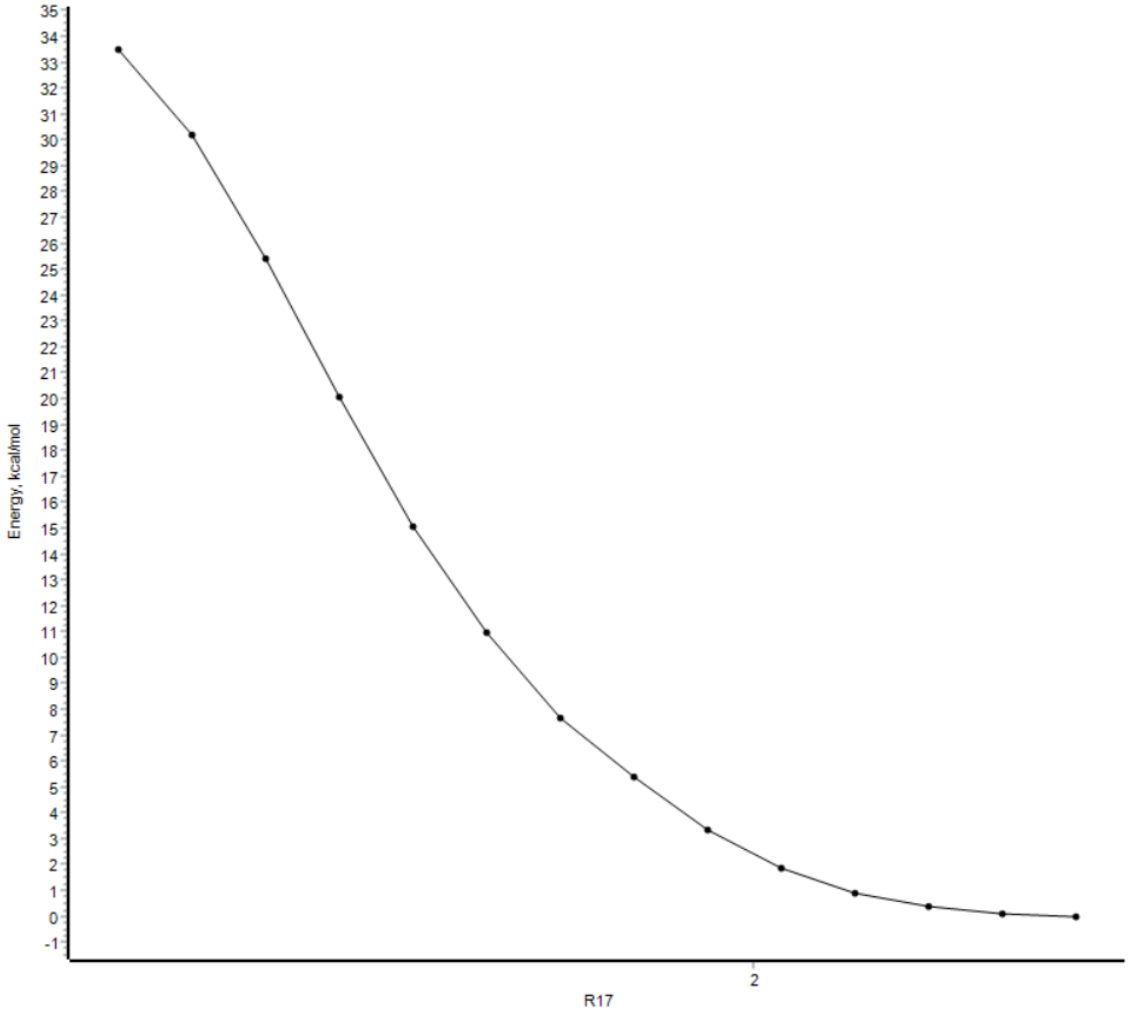

Figure S4. Scan on the C-H distance for the deprotonation of **A3_NEt3.**

3.3. Comparison of the N protonation versus Cl abstraction in A6.

The thermodynamics for the chloride abstraction from **A6** to form neutral rhodium complex together with $[HNEt_3]^+Cl^-$ contact ion pair (**A6_HNEt3Cl**) has been computed and compared to the protonation of the nitrogen to form **A7**. Formation of **A7** has been found to be thermodynamically more favorable than chloride abstraction.

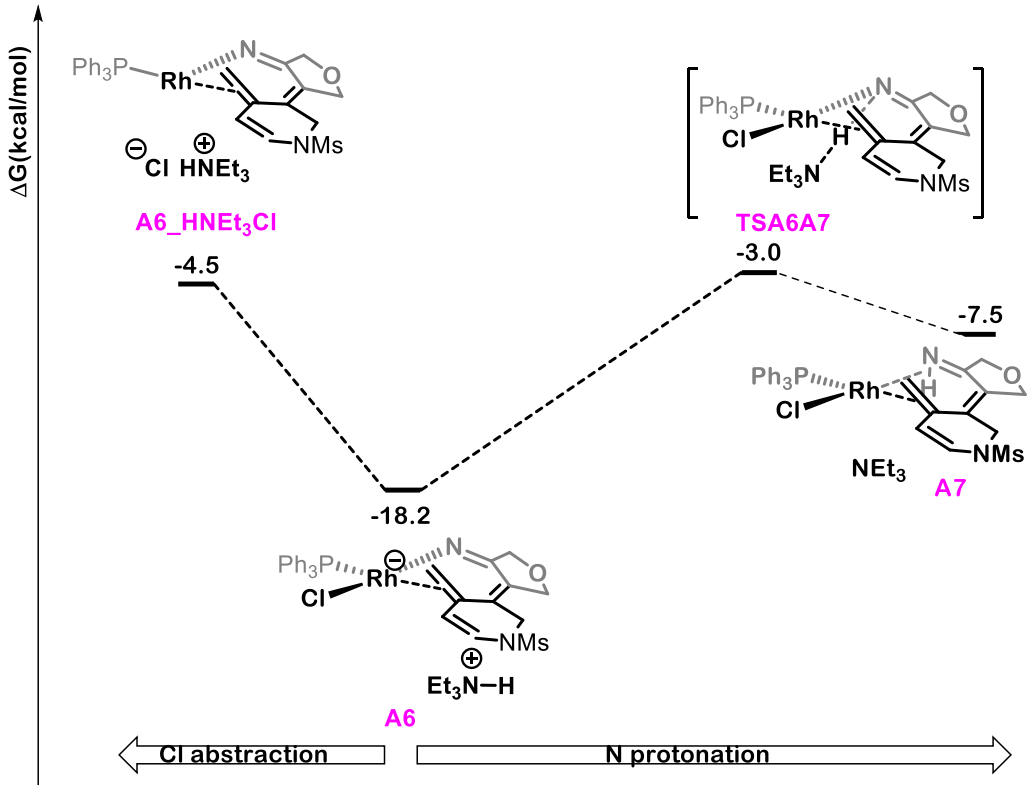

Figure S5. DFT calculations for the chloride abstraction from **A6** and comparison with nitrogen protonation through **TSA6A7.**

3.4. Comparison of the Rh-catalyzed versus Et_3N mediated deprotonation of A9.

Three different pathways for the deprotonation of **A9** have been evaluated (Figure S6). The rhodium-catalyzed pathway through **TSA9A10** was found to have a barrier of 23 kcal/mol. The triethylamine-mediated deprotonation of **A9**, with rhodium coordinated to the amine, was found to have a barrier of 33.4 kcal/mol. Conversely, the barrier for the triethylamine-mediated deprotonation on intermediate **A9'**, not coordinated to rhodium, could not be located. However, the **A9'_Et3N** adduct has already an energy of -36.9 kcal/mol (Figure S6), and a scan on the N-H distance (Figure S7) showed that the barrier is not lower than 175 kcal/mol. Thus, the triethylamine-mediated pathways were disregarded.

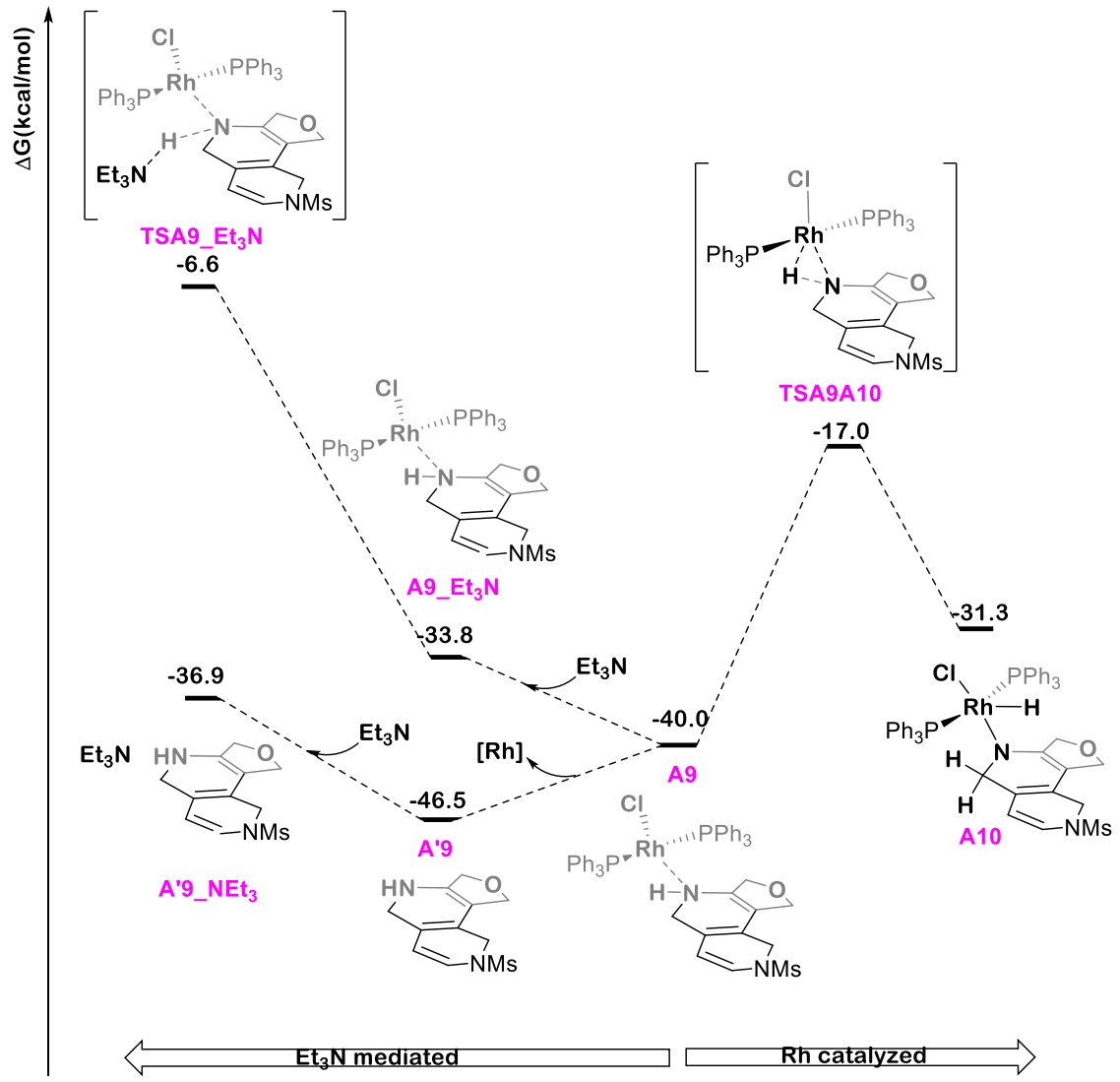

Figure S6. DFT calculations for the Et_3N mediated deprotonation of **A9** and comparison with the rhodium-catalyzed pathway through **TSA9A10.**

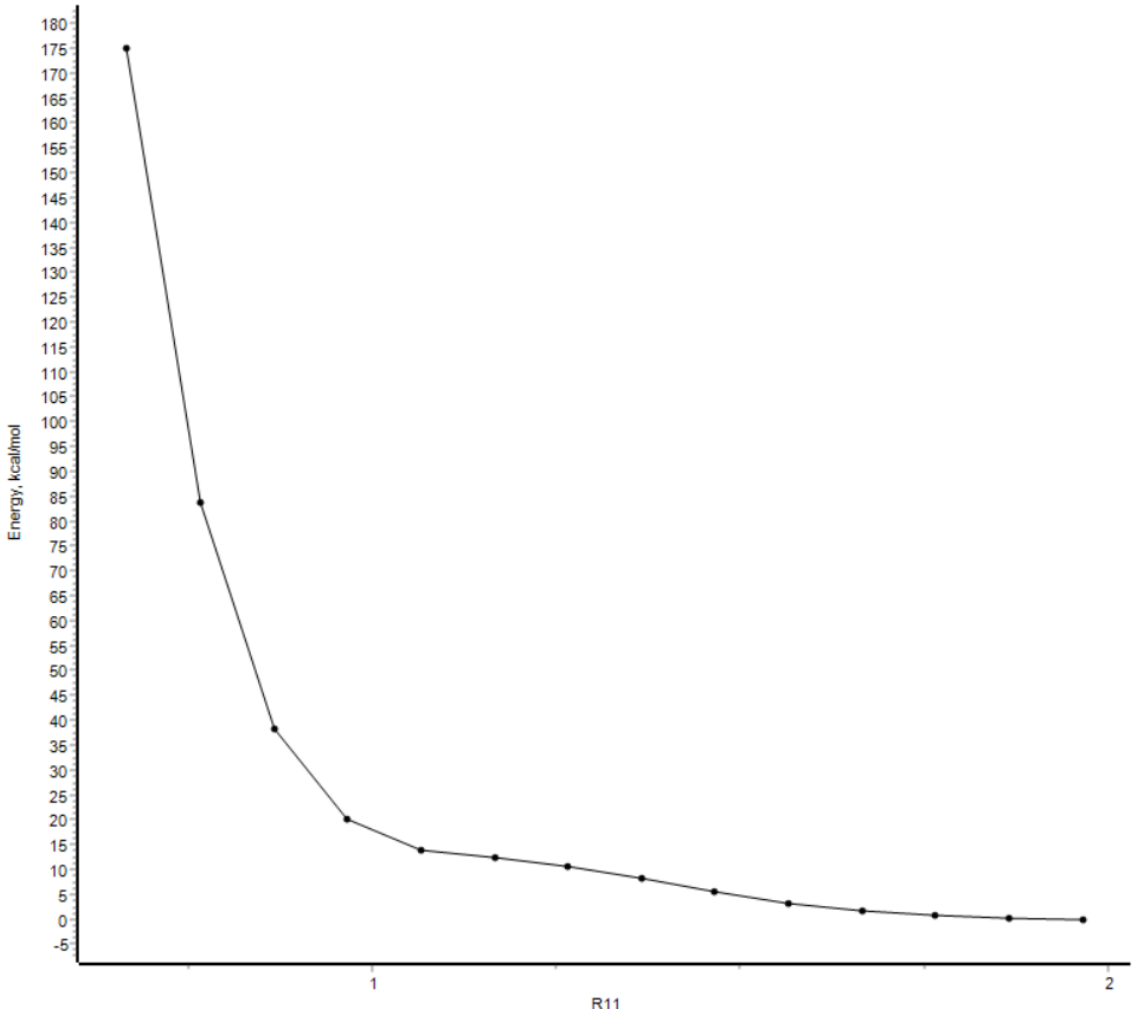

Figure S7. Scan on the N-H distance for the deprotonation of **A9'_NEt3.**

3.5. Computed energy profile for B pathway.

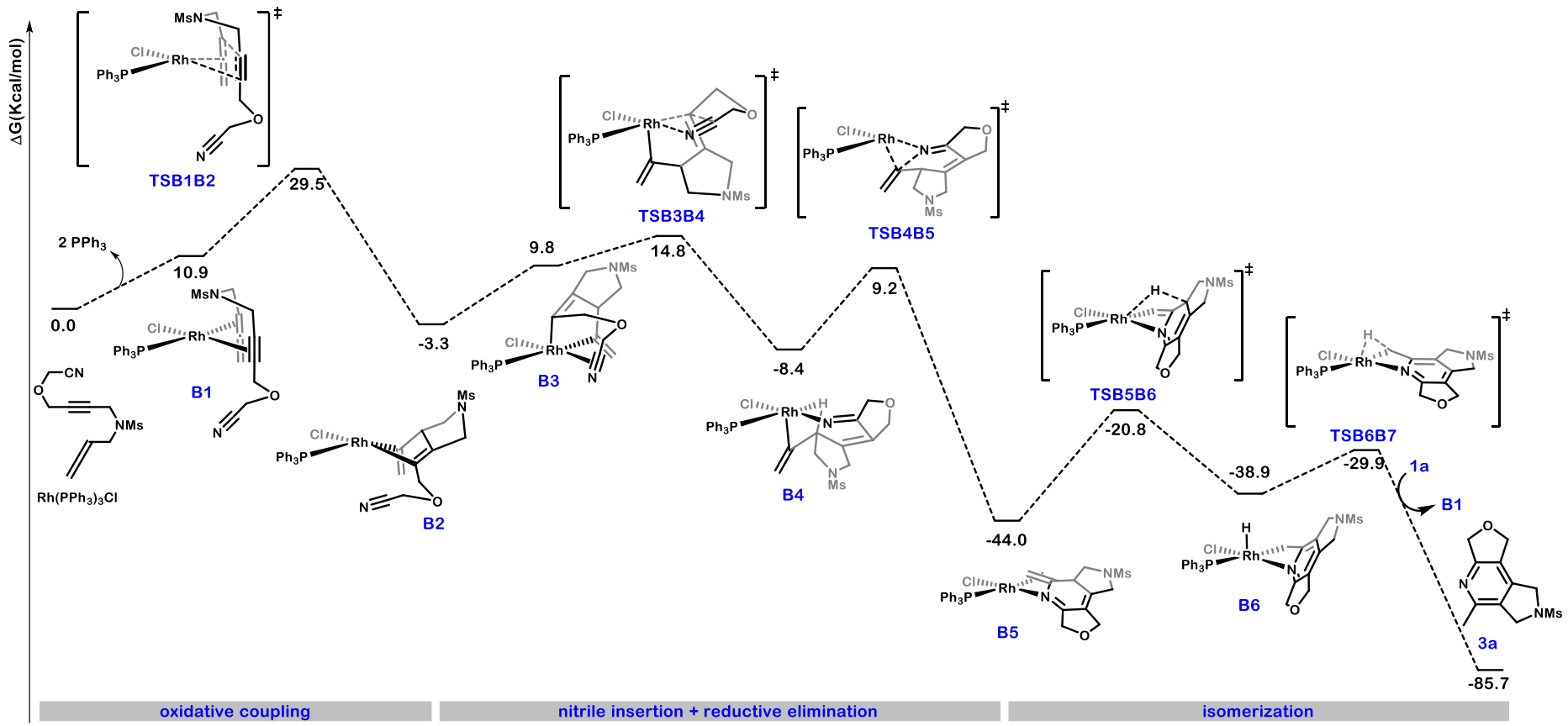

Figure S8. Gibbs energy for B pathway. Relative Gibbs energies (393.15 K) with respect to **1a** and [RhCl(PPh$_3$)$_3$] are shown in kcal/mol.

4. Molecular structures of A4, A4’ and substituted allenes A4Ext and A4Int

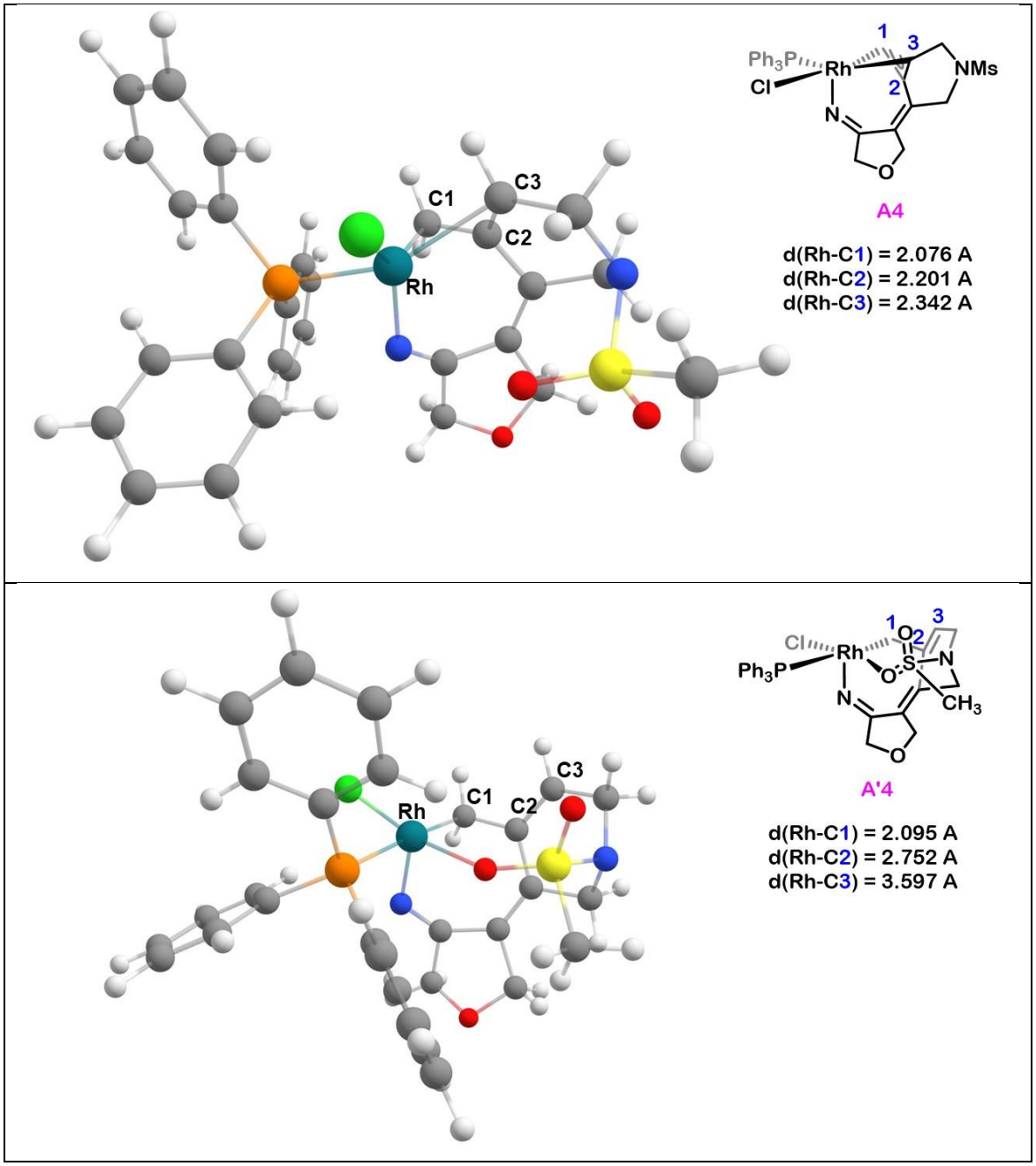

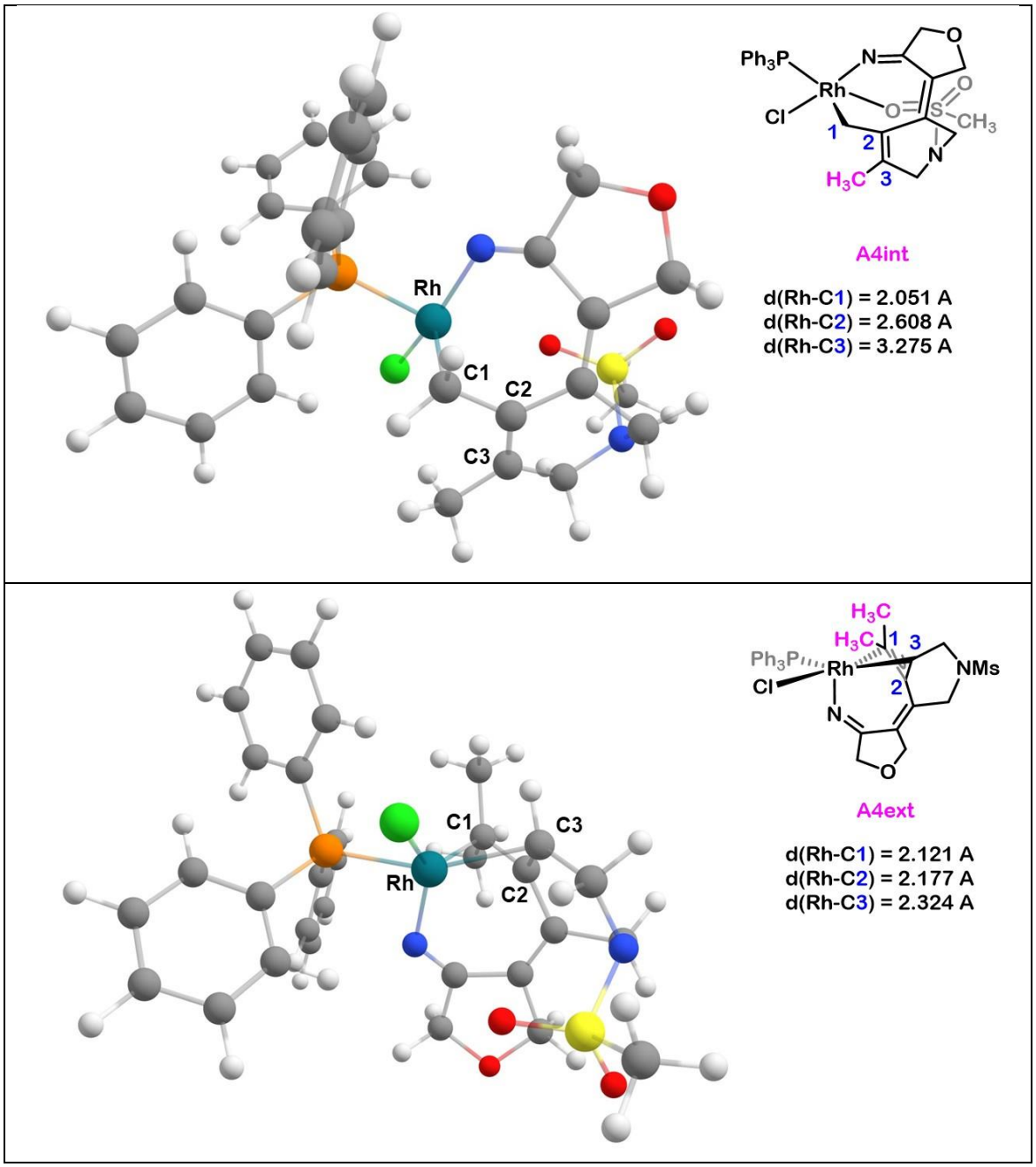

Figure S9. Molecular structure of intermediates **A4**, **A'4**, **A4int**, and **A4ext**; selected distances in Å.

5. Study of the steric difference between the internal and external allene carbons in A4 and A4'

	A4-Internal carbon	A4-External Carbon	A'4-Internal carbon	A'4-External Carbon
$\%V_{Bur}$	79 %	73.4 %	75.2 %	66 %

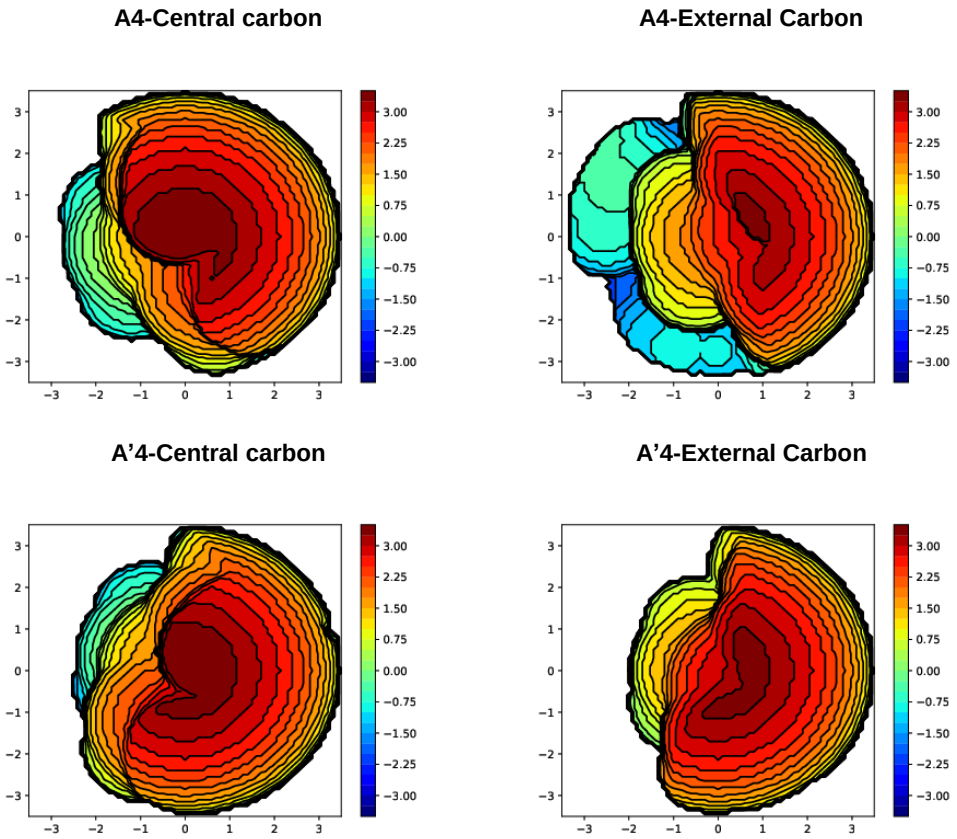

Figure S10. $\%V_{bur}$ values in the internal and external carbon of the allene for **A4** and **A'4**.